Peri- and intra-implant bone response to microporous Ti coatings with surface modification

Annabel Braem[a]

Amol Chaudhari[b],

Marcio Vivan Cardoso[b],

Jan Schrooten[a],

Joke Duyck[b],

Jozef Vleugels[a]

[a] Department of Metallurgy and Materials Engineering (MTM), KU Leuven, Kasteelpark Arenberg 44 – bus 2450, B-3001 Heverlee, Belgium

[b] Department of Oral Health Sciences, BIOMAT Research Group, KU Leuven, Kapucijnenvoer 7 blok a – bus 7001, B-3000 Leuven, Belgium

Received 23 July 2013, Revised 8 October 2013, Accepted 15 October 2013, Available online 22 October 2013

doi:10.1016/j.actbio.2013.10.017

Abstract

Bone growth on and into implants exhibiting substantial surface porosity is a promising strategy in order to improve the long-term stable fixation of bone implants. However, the reliability in clinical applications remains a point of discussion. Most attention has been dedicated to the role of macroporosity, leading to the general consensus of a minimal pore size of 50–100 μm in order to allow bone ingrowth. In this in vivo study, we assessed the feasibility of early bone ingrowth into a predominantly microporous Ti coating with an average thickness of 150 μm and the hypothesis of improving the bone response through surface modification of the porous coating. Implants were placed in the cortical bone of rabbit tibiae for periods of 2 and 4 weeks and evaluated histologically and histomorphometrically using light microscopy and scanning electron microscopy. Bone with osteocytes encased in the mineralized matrix was found throughout the porous Ti coating up to the coating/substrate interface, highlighting that osseointegration of microporosities (<10 μm) was achievable. The bone trabeculae interweaved with the pore struts, establishing a large contact area which might enable an improved load transfer and stronger implant/bone interface. Furthermore, there was a clear interconnection with the surrounding cortical bone, suggesting that mechanical interlocking of the coating in the host bone in the long term is possible. When surface modifications inside the porous structure further reduced the interconnective pore size to the submicrometer level, bone ingrowth was impaired. On the other hand, application of a sol–gel-derived bioactive glass–ceramic coating without altering the pore characteristics was found to significantly improve bone regeneration around the coating, while still supporting bone ingrowth.

Keywords

Porous Ti coatings; Microporosity; Bone ingrowth; Surface functionalization; Bioactive glass

---

1. Introduction

Joint replacement and dental restoration have evolved enormously over the past decades, resulting in excellent clinical success rates. Ten-year survival rates up to 95.3% for hip implants and even 98.8% for dental implants have been reported [1] and [2]. However, due to the ever-expanding demand for implants, an increasing number of patients still suffer from implant failure and, in addition, there is a trend towards a younger and more active patient population, which raises higher expectations regarding the durability and longevity of implants [3]. Maintaining a long-term stable fixation has become a key priority in implantology. In this regard, the concept of osseointegration gave rise to the development of cementless implants relying on a close implant/bone contact for a firm retention in the host bone. Although the first generation of cementless implants was not unambiguously successful, recent studies confirm a long-term survivorship for different cementless components comparable to their cemented counterparts [4] and [5].

Due to the outstanding mechanical properties such as a high strength and good fatigue resistance in combination with an excellent biocompatibility, titanium and Ti alloys have become the material of choice for load-bearing implant applications [6]. The stable oxide layer at the surface enables a close bone apposition, allowing successful osseointegration under appropriate conditions (implant surface, quality of the host bone, loading condition), but in order to improve outcomes in more challenging circumstances (e.g. compromised bone), further control of the bone formation is required.

From a materials perspective, the implant surface determines the rate and extent of osseointegration. Therefore, extensive research efforts focused on modifying the bioinert Ti surface towards an improved osteoconductivity or even osteoinductivity in order to stimulate a more efficient peri-implant bone formation [7], [8] and [9]. In a first approach, the surface topography was altered either on a macro- and microscale by surface roughening techniques (e.g. sandblasting and acid-etching), as a higher roughness promoted implant stability through an increased friction force with the bone, or on a nanoscale in order to encourage bone cell interactions [10], [11] and [12]. Secondly, chemical modification of the surface (e.g. calcium phosphate (CaP) or biomolecule coatings) could mimic the natural bone interface and even stimulated bone regeneration [12] and [13].

Porous Ti coatings, generally applied by plasma spraying or sintering of Ti particles, present a particular surface topography combining an increased surface roughness for improved initial implant stability with the potential to achieve long-term stability through mechanical interlocking at the implant/bone interface by bone ingrowth into the pores. The eventual bone anchorage, however, strongly depends on the quality (amount and interconnectivity) of osseointegration into the porous structure. This is primarily determined by the pore characteristics of the coating. Highly porous and interconnected open-cell structures favour bone ingrowth and the optimal pore size is generally accepted to be in the 100–400 μm range as a compromise to provide sufficient space for cell migration and vascularization, while maintaining the mechanical strength of the porous material [14], [15] and [16].

Modification of the Ti surface to improve the osseointegration of dense implants is well established; several recent studies have confirmed the beneficial effect of nanostructured surfaces [17] or CaP [18] and [19], calcium silicate and calcium titanate [20] based coatings whether or not doped with bioactive ions [21], [22] and [23] on bone formation. Surface modification of the internal pore surface of porous Ti constructs has been limited mostly to macroporous Ti scaffolds, showing an improved bone ingrowth after sand blasting and/or acid etching [24], acid–alkali treatment [25],

coating with CaP [26] or hydroxyapatite [27] or preparation of nanostructured calcium titanate and titanium oxide surfaces [28].

Recently, we developed a new processing route for porous Ti coatings with predominantly micropore sizes [29]. Few studies have considered the possible effect of microporosity (0.5–10 μm) on osseointegration and only recently research on CaP has shown that micropores in scaffold struts can be employed as additional space for bone ingrowth [30], [31] and [32]. Therefore, the first objective of the present study was to assess the early peri-implant tissue response to porous pure Ti coatings with significant microporosity. Secondly, it was hypothesized that biofunctionalization of the internal pore surface could improve the bone regeneration in the vicinity of the coatings. However, when envisaging the modification of the internal surface of a porous coating, direct line-of-sight techniques, such as plasma spraying, are not qualified. Wet chemical techniques based on a solution penetrating the entire porous structure are more suitable [9]. We proposed three wet chemical techniques for the application of an additional surface layer in the porous structure. Anatase TiO_2, which is known to enhance the bioactivity of Ti [33], was applied by a hydrothermal treatment (HT) [34]. Furthermore, micro-arc oxidation (MAO) was used to produce a TiO_2 surface layer containing Ca^{2+} and PO_4^{3-} ions [35]. Previous studies have shown that MAO coatings enhance the bone response for flat Ti substrates [36], especially when Ca^{2+} and PO_4^{3-} ions are incorporated in the surface layer [37] and [38]. Alternatively, Ca^{2+} and PO_4^{3-} ions can also be introduced in the form of dissolution products released from a bioactive glass (BAG) matrix [39]. Both melt and sol–gel-derived BAGs have proven to support bone bonding in vivo, but especially sol–gel BAG is associated with osteogenesis due to an increased release of ionic species from its intrinsically higher surface area [40] and [41]. Moreover, as sol–gel synthesis is more compatible with the coating of porous structures, this was the preferred processing route in this study [42]. Coated Ti implants were inserted in the rabbit tibia, applying a bone cavity model featuring a regeneration compartment [43]. Histological and histomorphometrical analysis of the bone response after 2 and 4 weeks was done using transmission light microscopy (LM) and scanning electron microscopy (SEM).

2. Materials and methods

2.1. Materials and characterization

As substrate material, commercially pure Ti (thickness 1 mm, grade 2, Goodfellow) was laser cut into discs 15.5 mm in diameter for the surface characterization and discs 4 mm in diameter as implant material for the in vivo experiment. Next, the discs were decontaminated by ultrasonically cleaning in acetone (Acros Organics) and rinsing in distilled water followed by acid etching in a 4 vol.% HF (40%, Riedel-de Haën) and 20 vol.% HNO_3 (60%, Chemlab) solution for 60 s. After excessive rinsing in distilled water, the samples were autoclave sterilized.

As the unmodified reference coating, a porous pure titanium coating was applied using electrophoretic deposition (EPD) of titanium hydride (TiH_2) powder suspensions followed by dehydrogenation and sintering in vacuum, as described elsewhere [29]. The coating will be referred to as EPD Ti. Subsequently, this coating was functionalized using three different additional treatments. First, a hydrothermal treatment (Jožef Stefan Institute, Slovenia) was applied creating a thin microanatase TiO_2 layer on the outer and inner surfaces of the porous Ti coating [34]. Alternatively, MAO (University of Bayreuth, Germany) was used to produce a pore filling TiO_2 layer containing Ca^{2+} and PO_4^{3-} ions [35]. Finally, a micrometer-thin bioactive glass coating was applied on the internal surface of the Ti coating using an all-alkoxide sol–gel synthesis (KU Leuven, Belgium) [42]. The samples are denominated EPD Ti + HT, EPD Ti + MAO and EPD Ti + BAG, respectively. Prior to implantation, the samples were sterilized either using an autoclave (EPD Ti and EPD Ti + HT) or by

heating to 200 °C in a vacuum furnace (EPD Ti + MAO and EPD Ti + BAG) in order to avoid dissolution of the functionalized coatings.

White light interferometry (WLI, Wyko NT 3300 Optical Profiler, Veeco Metrology Inc.) was used to obtain three-dimensional (3-D) roughness measurements. Ten spots divided over three different samples were measured per experimental surface. A quantitative analysis of the roughness data was performed using MountainsMapH Premium software (Digital Surf). Further qualitative analysis of the surface roughness was done by SEM (XL30-FEG, FEI).

The main pore structure characteristics (porosity, pore size, interconnecting pore channel (IPC) size) was done by mercury intrusion porosimetry (MIP, AutoPore IV 9500, Micromeritics) in combination with image analysis (PPM2OOF software, NIST) on SEM images of representative metallographic cross-sections.

2.2. Surgical procedure and tissue processing

The animal handling and experimental protocol used in this study was approved by the Animal Ethics Committee of KU Leuven and was performed according to the Belgian national legislation concerning the protection and wellbeing of animals. (Approval ID: P122/2008)

Six mature New Zealand white rabbits (average weight 3.17 ± 0.18 kg) underwent surgery as described elsewhere [43]. In short, following anaesthesia, four double-stepped cavities were drilled exclusively in the cortical bone of the diaphysis at the medial side of the proximal tibia. The outer step diameter was 4 mm in size for a press-fit mounting of the coated implants; the smaller inner cavity was 2 mm in diameter with a depth of 0.5 mm (Fig. 1a). To ensure a standardized blood supply to the cavity during healing, a perforation (0.5 mm diameter) to the bone marrow was made into the base of the cavity centre. Next, the sterilized implants were positioned into the outer cavity and covered by a Ti osteosynthesis plate fixed on the cortical bone by means of two Ti osteosynthesis screws (Nobel Biocare), to ensure a stable fixation of the implants. Each rabbit received a reference coated implant and the three functionalized coated implants, but only for one of both tibiae. After a healing period of 2 weeks, the above procedure was repeated for the other tibia, again allowing a healing period of 2 weeks. Both healing periods were randomly attributed to the left or right tibia of each animal, as were the sites of the various samples within the tibia.

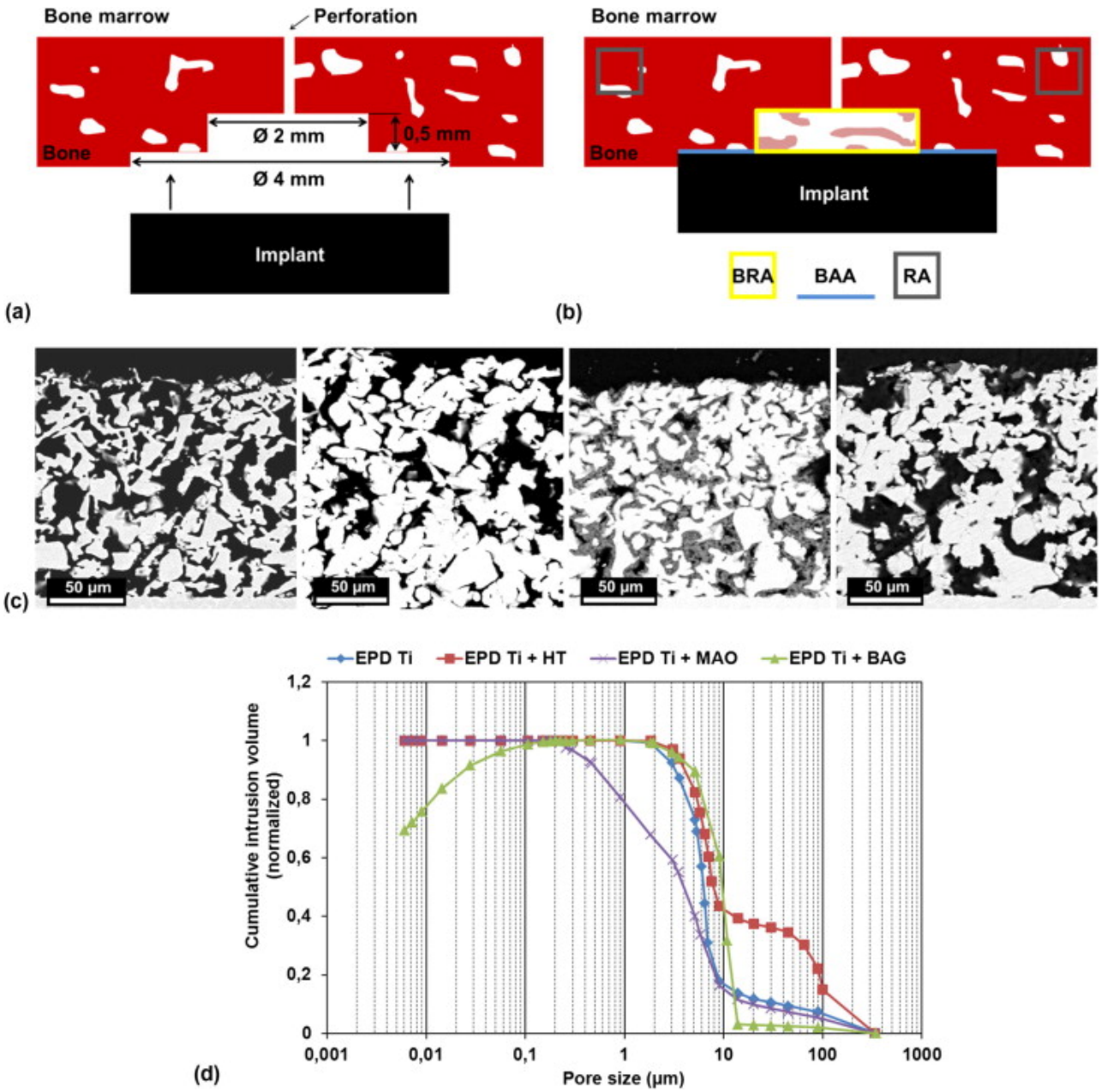

Fig. 1.

Schematic cross-section of (a) the implantation site and (b) the implant/bone assembly for histomorphometrical analysis. (c) BSE-SEM micrographs of representative cross-sections of EPD Ti, EPD Ti + HT, EPD Ti + MAO and EPD Ti + BAG respectively prior to implantation, and (d) the cumulative intrusion volume as a function of pore size as measured by mercury intrusion porosimetry.

Two weeks after the second surgery, the animals were euthanized and the tissues were further processed for analysis. The tibiae were dissected out and cut into bone blocks containing one implant. These blocks were fixed in a CaCO3 (p.a., VWR International) buffered formalin (35%, VWR International) solution during 3 days, dehydrated in a graded series of ethanol over 15 days and embedded in a methylmethacrylate (99.5%, VWR International) solution (containing 0.018% benzoyl peroxide as a catalyst) over 14 days at room temperature. Next, the bone blocks were cut

longitudinally and perpendicular to the implant surface using a diamond saw (Leica SP 1600, Leica Microsystems). The two most central sections of each implant were taken and prepared for either LM or SEM analysis. Sections were ground to a final thickness of ~30 μm using a micro-grinding system (Exakt 400 CS, Exakt) with an 800 grit SiC grinding paper (Hermes). To visualize both the mineralized bone and soft tissues using LM, the sections were surface stained with Stevenel's blue and counterstained with Von Gieson's picrofuchsin. For SEM analysis, the sections were further ground using a semi-automatic polishing machine (Pressair TF250, Jean Wirtz) with a 4000 grit SiC grinding paper (Hermes), followed by polishing with 3 μm diamond particles (Diapat S, VEM Metallurgie) on a neoprene cloth (OP-Chem, Struers).

2.3. Methods of analysis

The bone cavity model was the same as used by Chaudhari et al. [43]; Fig. 1b shows a schematic representation of a cross-sectioned implant/bone assembly. There are two main regions of interest, i.e., the central cavity, denominated as "bone regeneration area (BRA)", which is a region without any bone at the time of implantation and allows an investigation of the bone regeneration potential of the coating, and the periphery, the "bone adaptation area (BAA)", where the implant is initially in contact with the bone at the time of implantation and which allows the bone response in direct contact with the coating to be observed.

For a descriptive histological evaluation of the bone response, the surface stained sections were examined using LM. In addition, a quantitative histomorphometrical analysis was performed using image analysis software (Axiovision 4.0, Zeiss) with customized scripts for semi-automatic analysis. All analyses were performed by the same operator, who was blinded for the sample composition. As a measure for the bone regeneration potential, the bone area fraction (BAF), i.e. the percentage of the BRA occupied by newly formed bone trabeculae (BT), taking into account either the whole BRA cavity (BAF-500, in %), that part of the BRA within 100 μm from the implant (BAF-100, in %) or that part of the BRA at a distance of 100–500 μm from the implant (BAF-400, in %). To rule out any variability in bone density between different animals or even different positions in the cortical bone, all BAF parameters were considered proportional to the bone density measured in the reference areas (RA), well-defined areas next to the trauma zone reflecting the bone's natural density. In addition, the bone-to-implant contact ratios in the BAA (BIC-BAA, in %) or BRA (BIC-BRA, in %), were calculated as the percentage of the BAA length, respectively BRA length, in direct contact with bone. For the exact mathematical formulas, we refer to previous work [43].

Because the thickness of histological sections (~30 μm) is comparable to the pore size range of the EPD Ti coatings (2–50 μm), the coating's pore structure with or without ingrowth of bone cannot be representatively depicted by transmission LM due to projection artifacts. A surface-sensitive analytical technique such as SEM is preferred. Following gold coating with a sputtering device (Edwards S150), all samples were analysed with backscattered electron (BSE) imaging using the same operating conditions (10 mm working distance, 20 kV accelerating voltage) and image settings (contrast, brightness). Additionally, elemental analysis was done by SEM with associated energy dispersive X-ray spectroscopy (EDS, EDAX), while elemental mapping was performed using electron microprobe microanalysis (EPMA, JXA-8503F, JEOL Ltd) with associated wavelength dispersive X-ray spectroscopy (WDS). As histomorphometrical parameter, the percentage of the available pore area occupied by newly formed bone, i.e. the bone ingrowth fraction (BIF, in %), was determined by image analysis (CTAn, SkyScan NV). Validation of this protocol for histomorphometrical analysis was done by comparing the results for BAF-500 obtained by both LM and SEM (R2: 0.9826).

2.4. Statistical analysis

Significant differences ($P < 0.02$) in roughness and pore characteristics were identified by an unpaired Student's t-test using statistical analysis add-in software for Microsoft Excel® (Analyse-it® version 2.26, Analyse-it Software Ltd). The validity of the test was verified by checking the normality of distribution (Shapiro–Wilk). The equality of variances was investigated using an F-test ($P < 0.05$) and in the case of unequal variances, a Welch's correction was applied to the t-test.

Statistical analyses of the histomorphometrical parameters were performed with SAS 9.2 (SAS Institute Inc.). Because of the clustered nature of the data, a mixed statistical model considering both fixed effects (implant type and implant/time interaction) and random effects (animal) was applied. Normality of the data and homogeneity of the residuals were checked by diagnostic plots and if necessary, data were transformed to meet both requirements. The proc mixed option in SAS allowed to calculate the differences between implants for a certain healing period as well as the evolution over time (2 to 4 weeks) for a given implant type ($P < 0.05$ was considered to be statistically significant).

3. Results

3.1. Coating characterization

A quantitative 3-D topographical analysis (Table 1) was performed by the calculation of average roughness (Sa, amplitude parameter), texture aspect ratio (Str, spatial parameter) and developed interfacial area ratio (Sdr, hybrid parameter). Sa was comparable for all coatings in the absence of a directional structure (Str), whereas the surface area decreased when applying MAO or BAG coatings on EPD Ti. Representative cross-sections of the different coatings obtained by SEM (Fig. 1c) allowed us to calculate the overall porosity (Table 1), while the cumulative intrusion volume as obtained by MIP allowed us to establish an IPC size distribution (Fig. 1d). HT and BAG treatments did not significantly alter the original EPD Ti porosity value of ~50% and also the IPC size distribution was fairly comparable to EPD Ti, especially for the bulk pores (<10 μm). For the pore size range from 300 down to 10 μm, which can mainly be associated with the surface pores, the pore size distribution for EPD Ti + HT indicated a larger fraction of pores, probably due to surface cracks present in those samples. The strong deviation seen for EPD Ti + BAG at low pore sizes (<0.1 μm) was most probably due to an undesirable reaction between the Hg and the BAG during analysis, forming amalgams with several metals, as there is sodium [44]. MAO treatment on the other hand introduced a pore-filling Ti-oxide phase (grey phase in Fig. 1c), reducing the porosity to 28.0%. This was mainly reflected by a reduction of the bulk pore size shifting to the submicrometer range.

Table 1.

Surface roughness parameters of the different coatings measured by white light interferometry [29] and [52] (values represent mean ± SD).

	Sa (μm)	Str (−)	Sdr (%)	Porosity (%)
EPD Ti	4.5 ± 0.4	0.6 ± 0.1	61.7 ± 15.4	51.2 ± 3.9
EPD Ti + HT	4.9 ± 2.0	0.7 ± 0.1	56.9 ± 27.2	45.9 ± 1.0
EPD Ti + MAO	4.3 ± 0.2	0.8 ± 0.1	35.6 ± 9.9[a]	28.0 ± 3.8[a]
EPD Ti + BAG	4.3 ± 1.6	0.8 ± 0.1	40.5 ± 11.1a	51.3 ± 3.4

Sa = Roughness average, arithmetic mean of the absolute values of the surface departures from the mean plane.

Str = Texture aspect ratio, measure for the texture strength: values >0.5 suggest an isotropic texture; values <0.3 indicate a directional structure.

Sdr = Developed interfacial area ratio, percentage of additional surface area as compared to an ideal plane the size of the sampling area.

[a] Statistically significant differences with the unmodified EPD Ti surface.

3.2. Clinical observation

All rabbits remained in good health for the whole duration of the healing period. During implant retrieval, no clinical signs of infection or adverse tissue reaction were observed around the surgical site. In total, 48 implants were harvested and considered for further analysis.

3.3. Histology

Fig. 2 displays representative features of the tissue response after both 2 and 4 weeks of implantation obtained by LM. After 2 weeks of implantation (Fig. 2a and b), a non-organized connective tissue comprising osteoblast-like cells, adipocytes and accumulations of blood cells was observed as well as well-organized tissue consisting of blood cells organized into blood vessels, clusters of cuboidal shaped (i.e. active) osteoblast cells surrounded by osteoid deposition in connection with mineralized bone trabeculae. After 4 weeks (Fig. 2c), the bone trabeculae became more dense with smaller osteocyte lacunae and were covered with a row of active osteoblasts, suggesting an active bone formation process. Simultaneously, Fig. 2d depicts a multinucleated osteoclast at the interface between implant and original cortical bone in the BAA, demonstrating a process of bone resorption. This was found to be more pronounced after 4 than after 2 weeks of implantation.

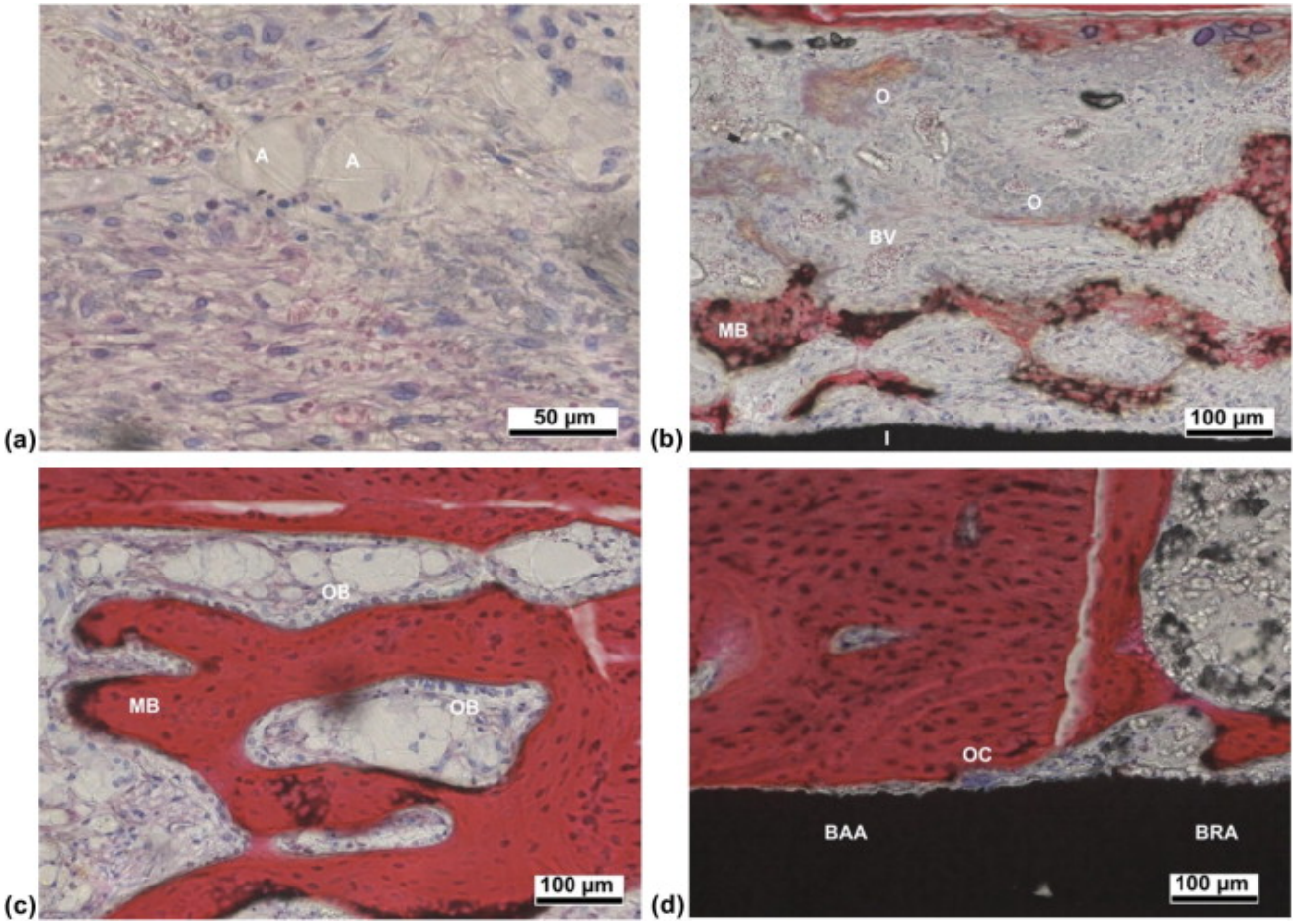

Fig. 2.

Detailed light micrographs of representative features of the histological observations: (a and b) non-organized connective tissue comprised of adipocytes (A), osteoblast-like cells and blood cells together with well-organized tissue of blood vessels (BV), active osteoblasts (OB) depositing osteoid (O) and mineralized bone (MB) after 2 weeks of implantation; (c) active OB lined up along dense MB and (d) multinucleated osteoclast (OC) at the interface between implant (I) and original cortical bone, illustrating bone remodelling, after 4 weeks of implantation.

Since visualization of bone in or in close contact with the microporous Ti coatings at high magnification was not possible using LM (due to projection artifacts) or X-ray computed tomography (due to scatter artifacts), BSE-SEM images were taken. As BSE images depict an atomic number contrast, the Ti implant and coating appeared bright (white), while the mineralized bone was grey. Discrimination between the low density organic soft tissue and the embedding medium was not possible using BSE and these materials are viewed as black areas. Observations of the mineralized bone trabeculae in the BRA above the Ti coatings were in accordance with LM. At 2 weeks, bone trabeculae were irregular and highly cellular, i.e., with a high proportion of osteoblast lacunae, whereas the bone trabeculae after 4 weeks occupied a larger part of the BRA and had become larger and more dense, i.e. smaller osteoblast lacunae (results not shown). In general, bone ingrowth into the coatings after 2 weeks was limited to the colonization of the open surface pores (Fig. 3a), although a low-mineralized tissue could be seen throughout the whole coating thickness in some samples (Fig. 3b).

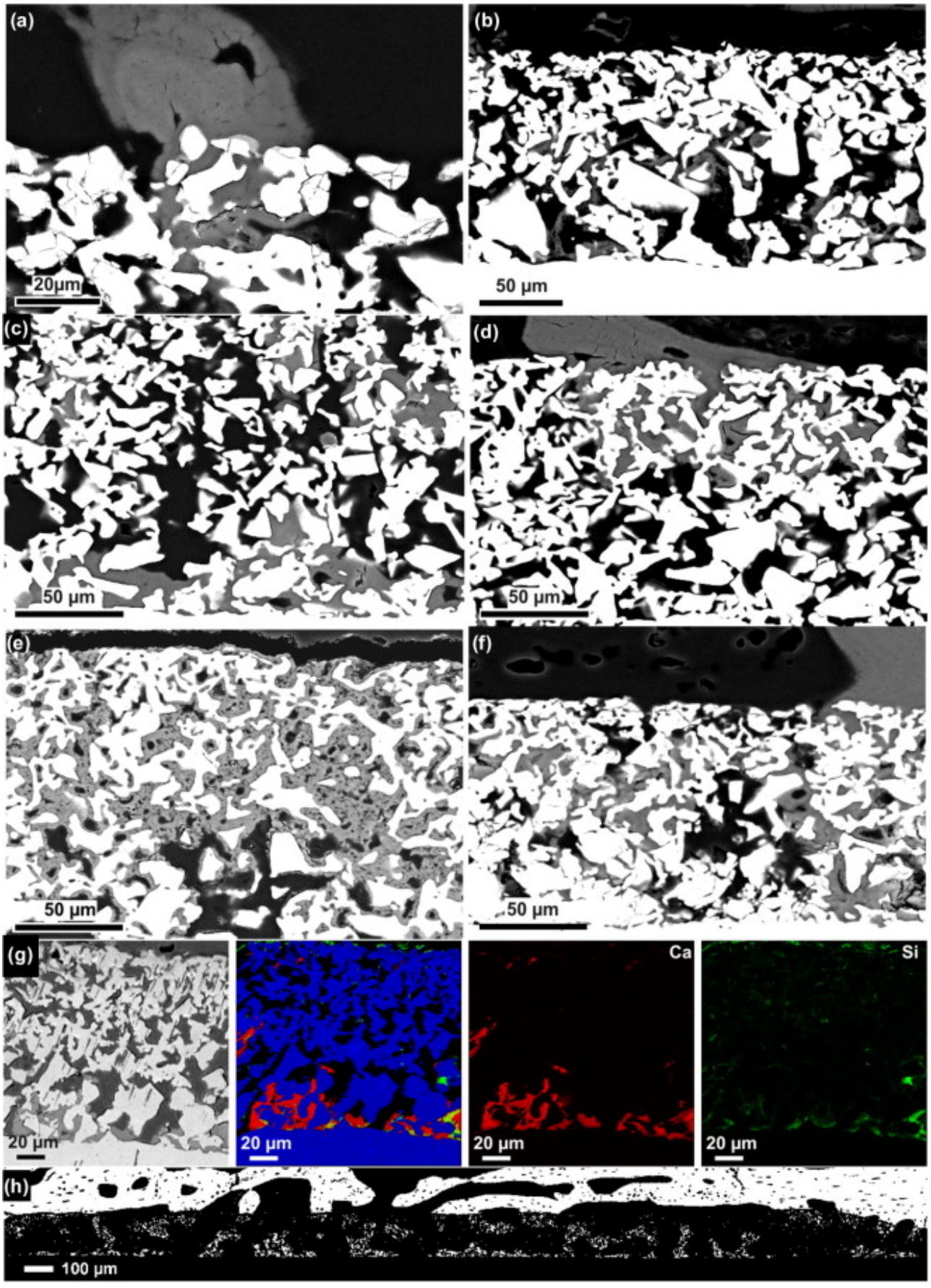
(a)
20μm
(b)
50 μm
(c)
50 μm
(d)
50 μm
(e)
50 μm
(f)
50 μm
(g)
20 μm
20 μm
Ca
20 μm
Si
20 μm
(h)
100 μm

Fig. 3.

(a and b) Representative BSE-SEM micrographs of a porous Ti coating cross-section after 2 weeks of implantation, indicating (a) limited bone ingrowth at the coating surface and (b) the presence of a low-mineralized phase throughout the whole coating. (c–f) Representative BSE-SEM micrographs of (c) EPD Ti, (d) EPD Ti + HT, (e) EPD Ti + MAO and (f) EPD Ti + BAG after 4 weeks of implantation, showing bone ingrowth up to the substrate/coating interface, except for EPD Ti + MAO. (g) BSE-SEM micrograph and associated WDS elemental mappings for Ti (blue), Ca (red), Si (green) of EPD Ti + BAG after 4 weeks of implantation. (h) Binarized BSE-SEM micrograph for EPD Ti after 4 weeks of implantation.

Fig. 3c–f shows representative BSE-SEM micrographs of cross-sections of the different coatings in contact with the BRA after 4 weeks of implantation. For EPD Ti + HT + BAG, the grey phase present throughout the whole coating (white) up to the coating/substrate interface was confirmed to be bone (with a Ca/P ratio of ca. 1.6) by EDS point analyses. Note that also osteocyte lacunae could be observed inside the coating. For EPD Ti + MAO, elemental analysis assigned the observed grey phase to a phosphated TiO2 phase which was already present prior to implantation (Fig. 1c). No significant differences in porosity, as determined by image analysis, could be observed between 2 and 4 weeks of implantation, indicating that no or only slow dissolution of the TiO2 phase had occurred.

For the EPD Ti + BAG coatings, traces of an additional grey phase, containing Si with small amounts of P, Ca and Na, were observed, pointing at the presence of partially dissolved BAG. To determine to what extent BAG was still remaining after implantation, a WDS elemental mapping was performed on a coating after 4 weeks of implantation (Fig. 3g). While Ca and P were the main composing elements of the prominent grey phase observed by BSE-SEM, Si (and thus BAG) was mainly detected as a thin layer at the coating surface (top) and coating/substrate interface (bottom), in contact with the new bone phase.

Additionally, the growth pattern of the bone trabeculae inside the porous coatings was visualized by binarizing BSE-SEM images in order to convert the bone phase to white and all other phases including the implant to black. A representative EPD Ti reference coating after 4 weeks of implantation is shown in Fig. 3h. This again confirmed that bone was present throughout the whole coating thickness, and also showed that bone appeared in the form of trabeculae, which are interconnected with the bone trabeculae in the BRA above or surrounding cortical bone inside the porous structure.

3.4. Histomorphometry

Fig. 4 summarizes the results of the histomorphometrical analysis. The fraction of newly formed bone with respect to the entire BRA, BAF-500 (Fig. 4a), tended to increase with implantation time for all functionalized coatings in comparison to the reference coating. However, a statistically significant difference was only observed for the EPD Ti + HT and EPD Ti + BAG between 2 and 4 weeks and more importantly when comparing EPD Ti + BAG (61.8 ± 5.6%) with the EPD Ti reference (36.3 ± 8.6%) at 4 weeks. In the vicinity of the implant, the effect of implantation time was more pronounced (BAF-100, Fig. 4b), but no significant differences could be seen among the various coatings. BAF-100 after 4 weeks was significantly higher than BAF-400 (Fig. 4c) for EPD Ti (49.8 ± 8.6% vs. 33.1 ± 9.0%) and EPD Ti + MAO (65.1 ± 7.0% vs. 45.9 ± 10.9%), whereas it was significantly lower than BAF-400 for EPD Ti + BAG (50.4 ± 4.5% vs. 64.8 ± 7.2%). A trend of increased BIC-BRA between 2 and 4 weeks of implantation can was observed, except for EPD Ti + BAG, for which the BIC-BRA at 4 weeks was significantly lower than for other conditions (Fig. 4d). As the bone remodelling cycle in the rabbit takes up to 6 weeks [45], the results for the BIC-BAA 2 and 4 weeks following implantation (data not shown) did not allow us to discriminate between the different coatings.

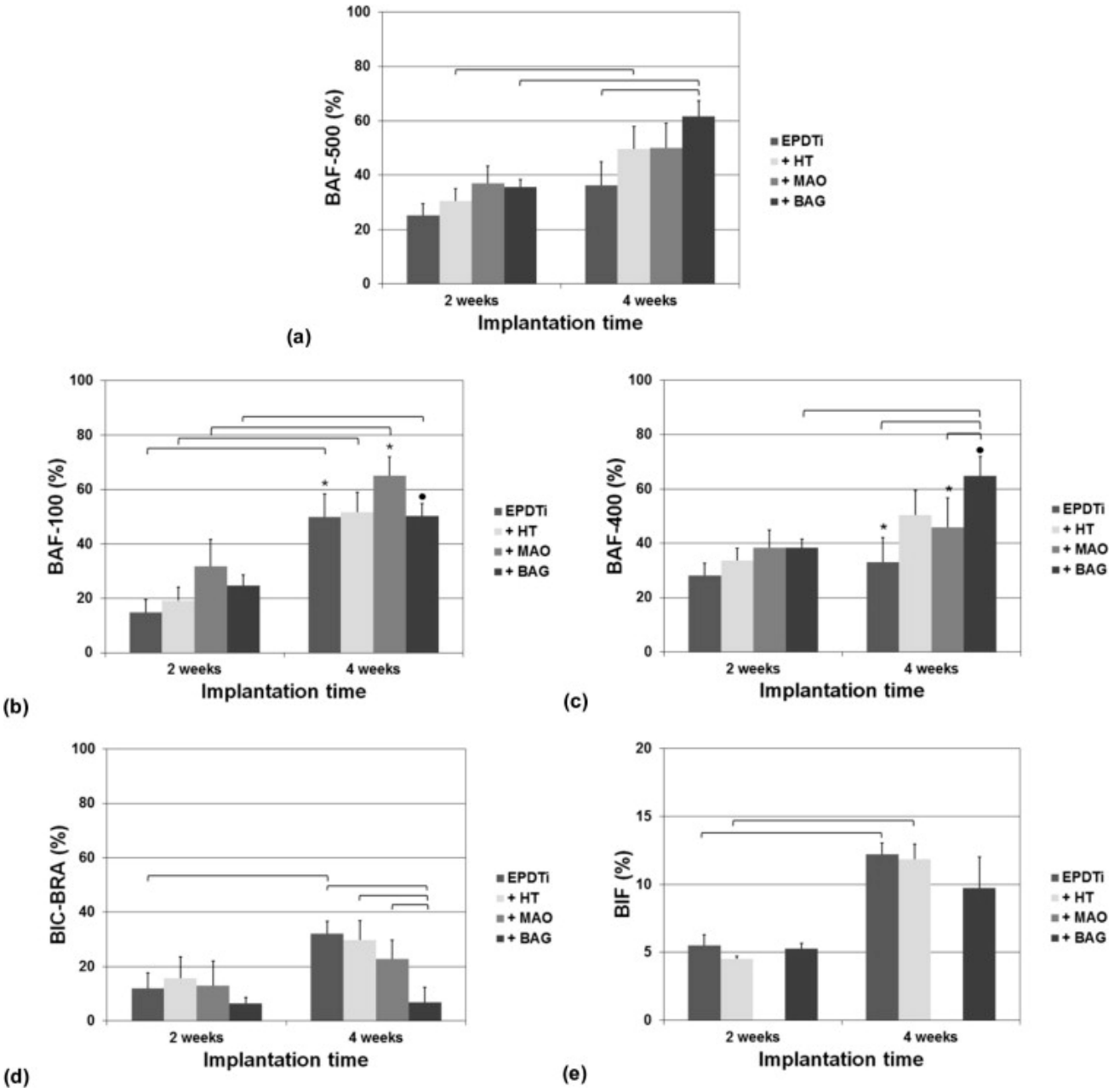

Fig. 4.

Bone histomorphometrical parameters: bone area fraction (BAF) (a) with respect to the entire bone regeneration area (BRA), BAF-500, or (b) with respect to the part of the BRA within 100 µm of the implant, BAF-100, or (c) with respect to the part of the BRA within 100 to 500 µm away from the implant, BAF-400, (d) bone-to-implant contact (BIC) in the BRA and (e) bone ingrowth fraction (BIF) in the different porous Ti coatings. Results are presented as mean values ± standard errors; statistically significant ($P < 0.05$) differences are indicated by the horizontal lines. ∗ and ● indicate statistically significant ($P < 0.05$) differences between BAF-100 and BAF-400 for the same coating and implantation time.

The BIF, i.e. new bone established inside the porous Ti coating, tended to increase over time, except for EPD Ti + MAO, where no bone ingrowth was observed (Fig. 4e). However, for a specific implantation period, no differences could be observed among the various conditions.

4. Discussion

Porous Ti coated implants have already been successfully applied in both orthopaedics and dentistry [3], [46], [47], [48] and [49]. However, in certain specific circumstances such as the application in compromised bone or in revision surgery, the fixation results are still suboptimal [50]. Additionally, higher patient demands, such as an improved implant durability and longevity for younger patients and/or a reduced recovery period, necessitate a progressive increase in quality and speed of osseointegration.

Current clinically applied porous Ti coatings are mainly limited to coatings obtained by plasma spraying techniques, such as vacuum plasma spraying (VPS). These coatings benefit from a moderate to high surface roughness (a few μm up to 100 μm), allowing a good retention in the host bone, but possess an irregular porosity distribution and limited pore interconnectivity [15] and [51]. In the context of bone ingrowth, these coatings should mostly be considered as roughened surfaces rather than porous coatings. In contrast, porous Ti coatings obtained by powder sintering can be fully interconnected with a well-controlled porosity [15]. The porous Ti coatings used in this study combine an increased porosity with a good mechanical strength, while significantly reducing the risk of biofilm formation as compared to VPS Ti coatings [29] and [52]. However, the predominantly microporous structure (Fig. 1d) rendered their potential for bone ingrowth applications uncertain, as the general consensus in literature is on a minimal pore size of 50 to 100 μm [14], [15] and [16]. Bone ingrowth in micropores (0.5–10 μm) [30] has only been addressed in a limited number of studies. For CaP materials, for example, although the presence of micropores has been reported earlier to positively influence bone formation in macropores [30], [53], [54] and [55], Levengood et al. were the first to exploit microporosity as additional space for bone ingrowth [30]. For titanium, the focus is still on macroporosity, but bone ingrowth in pores down to 50 μm has been demonstrated [56], [57] and [58]. However, it should be noted that studies often only cite the average pore size, while it is actually the smaller IPC size that limits bone ingrowth. Baril et al. recently found that bone ingrowth in porous Ti structures appeared for interconnective sizes as small as 28 μm [59]. The observation of bone growth into the microporous coatings presented in this study (Fig. 3) extends this lower limit further to the microporosity size range below 10 μm. Bone and even osteocytes embedded in a mineralized matrix are present in the micropores, similarly to what Levengood et al. reported for CaP scaffolds [30]. This can be observed for chemically modified EPD Ti as well as for the unmodified reference coating, indicating that osteogenic cells migrated through the microporous Ti structure and produced mineralized tissue even in the absence of a surface modification. Visualizing the patterns of bone ingrowth (Fig. 3h) revealed that the bone grows as trabeculae through the microporous structure, interwoven with the pore struts. This leads to a strong increase in contact area, which may lead to a more uniform load transfer and a stronger implant/bone interface. Moreover, the ingrown bone was clearly interconnected with the surrounding cortical bone, confirming the possibility of mechanical interlocking of the implant in the host bone tissue. As the coating thickness was less than 200 μm, it is likely that bone cells inside the porous structure remained close enough to a vascular supply in the surrounding bone tissue to retain access to nutrients and expel waste [30]. This could also explain the discrepancy with the literature consensus on a 100 μm minimal pore size. Generally, the focus in bone regeneration research has been on larger porous structures (>200 μm) such as scaffolds, where macroporosity is indeed required for vascularization.

In addition to assessing the possibility of bone ingrowth in microporous Ti coatings, the second objective of this study was to investigate the effect of surface modifications on bone healing around and inside the porous coatings. In order to modify the internal surface of the microporous Ti

coatings, three wet chemical techniques were selected which are known to enhance bone response on dense Ti substrates.

Histological observations confirmed the presence of normal bone healing patterns for all coatings. Bone regeneration in the BRA evolved from unorganized connective tissue (Fig. 2a) over osteoid depositing osteoblasts to newly formed bone trabeculae aligned with active osteoblasts (Fig. 2b and c), while osteoclast activity in the BAA after 4 weeks (Fig. 2d) indicated bone remodelling, an elementary phase of osseointegration. Both size and density of the bone trabeculae increased with implantation time (Fig. 2c), an observation that was supported by the histomorphometrical results (Fig. 4a–c). Increased bone regeneration in the BRA, which is insignificant for HT and MAO coatings, could be observed for BAG coatings when compared to the unmodified EPD Ti coating (Fig. 4a), confirming the osteogenic potential of this sol–gel-derived glass–ceramic coating. However, similarly to what has been observed for a melt-derived glass–ceramic coating [43], this enhanced bone regeneration was due to an increased bone fraction further away from the surface (BAF-400) rather than at the implant surface (BAF-100) (Fig. 4b and c). In relation to this, the BIC-BRA was significantly lower for EPD Ti + BAG when compared to EPD Ti. The bioactive nature of BAG is related to its gradual dissolution in contact with physiological fluids, which induces osteoconduction by the formation of a HCA layer on the surface and promotes osteoinduction by the leaching of degradation products [41] and [60]. It has been shown that the ionic degradation products of sol–gel-derived BAG have a beneficial effect on osteoblasts [40]. However, this ion leaching (cations such as Ca^{2+} and Na^{+}) has also been found to increase the interfacial pH, which was suggested to decrease cell attachment [41] and [61]. This may explain the improved BAF-500, in combination with a limited BIC-BRA.

Bone ingrowth after 2 weeks remained limited to the open surface pores, whereas bone was found throughout the whole coating thickness up to the coating/substrate interface for EPD Ti + HT or BAG after 4 weeks (Fig. 3), similarly to what was observed for the unmodified EPD Ti reference coating. BIF slightly increased with the duration of implantation, but did not allow us to discriminate between the different surface modifications. This was in line with the results for bone regeneration close to the implant surface (BAF-100), which was similar for the EPD Ti reference coating before and after HT or BAG treatment. Within the short time frame of this study, these surface modifications did not seem to contribute to a significantly improved bone ingrowth into the porous Ti coatings. However, it is to be noted that prolonged in vivo experiments should be implemented to further elucidate the effect on the eventual osseointegration, especially in the case of BAG, since a faster bone regeneration around the coating was clearly established. For EPD Ti + MAO, no bone was observed inside the pores, which only contained the original pore filling TiO_2 phase (Fig. 3c). This is explained by the differences in pore characteristics (Fig. 2c and d). Whereas for EPD Ti + HT or BAG the IPC size range was comparable to that of the unmodified EPD Ti coating, it was shifted towards the submicrometer level for EPD Ti + MAO, which is probably too small to allow colonization by osteoblasts. This emphasizes the importance of a surface modification which does not drastically alter the pore structure of the coatings.

5. Conclusion

The experimental data demonstrated that bone cells populate the pore structure of the experimental EPD Ti coatings, enabling bone ingrowth into the pores. This shifts the lower threshold value for pore sizes, allowing bone ingrowth towards the microporosity range below 10 μm. Moreover, the bone trabeculae were strongly interwoven with the pore struts and the well-established interconnections with the surrounding cortical bone suggest that micro-interlocking of the porous coating is possible, which can be a major advantage for the long-term stability of implants. When envisaging surface

modifications to further improve the osteoconductivity of the porous Ti, pore sizes should not be further reduced, as this would obstruct bone ingrowth, as could be observed after MAO of the porous Ti. It is therefore advisable that the processing parameters are fine-tuned in order to minimize the effect on the pore characteristics.

A sol–gel-derived bioactive glass–ceramic in the inner pore surface of the EPD Ti coating, which did not alter the pore structure, was shown to allow bone ingrowth comparable to the unmodified reference, while significantly increasing the bone regeneration around the porous coatings. The bone-to-implant contact, however, was reduced, indicating the necessity of tuning the BAG surface properties. Similarly, hydrothermal treatment did not interfere with bone ingrowth in the porous Ti coating; however, no significant improvement in bone regeneration was observed.

Acknowledgements

This work was supported by the 6th and 7th Framework Programmes of the Commission of the European Communities under project contract No. NMP3-CT-2006-026501 (MEDDELCOAT) and 278425 (COATIM), and the Research Fund of KU Leuven under projects IDO/06/013 and GOA/08/007 and the knowledge platform IOF/KP/11/007. Gratitude is extended to the Civil Engineering Department of KU Leuven and Dr. ir. Bram Neirinck (Department of Metallurgy and Materials Engineering, KU Leuven) for mercury intrusion porosimetry measurements and to Prof. Monika Willert-Porada and Dipl.-Ing. Andreas Rosin of the University of Bayreuth (Germany) and Prof. Saša Novak and Dr. Nataša Drnovšek of the Jožef Stefan Institute (Slovenia) for the implementation of the Ti surface modifications. We gratefully acknowledge support from the Hercules Foundation (project ZW09-09) and ir. Tom Van der Donck for the EPMA analysis.

Appendix A. Figures with essential colour discrimination

Certain figures in this article, particularly Figs. 1–3, are difficult to interpret in black and white. The full colour images can be found in the on-line version, at http://dx.doi.org/10.1016/j.actbio.2013.10.017.

References

[1]

Data obtained from the Swedish Hip Arthroplasty Register: Annual report 2011. Online. 2013 April. Available from URL: http://www.shpr.se.

[2]

D. Buser, S. Janner, J.-G. Wittneben, U. Brägger, C.A. Ramseier, G.E. Salvi. 10-Year Survival and success rates of 511 titanium implants with a sandblasted and acid-etched surface: a retrospective study in 303 partially edentulous patients. Clin Implant Dent Relat Res, 14 (2012), pp. 839–851.

[3]

A. Eskelinen, V. Remes, I. Helenius, P. Pulkkinen, J. Nevalainen, P. Paavolainen

Total hip arthroplasty for primary osteoarthrosis in younger patients in the Finnish arthroplasty register

Acta Orthop, 76 (2005), pp. 28–41

[4]

C.J. Della Valle, N.W. Mesko, L. Quigley, A.G. Rosenberg, J.J. Jacobs, J.O. Galante

Primary total hip arthroplasty with a porous-coated acetabular component

J Bone Joint Surg, 91 (2009), pp. 1130–1135

[5]

K. Corten, R.B. Bourne, K.D. Charron, K. Au, C.H. Rorabeck

What works best, a cemented or cementless primary total hip arthroplasty?

Clin Orthop Relat Res, 469 (2011), pp. 209–217

[6]

M. Geetha, A.K. Singh, R. Asokamani, A.K. Gogia

Ti based biomaterials, the ultimate choice for orthopaedic implants – a review

Prog Mater Sci, 54 (2009), pp. 397–425

[7]

A. Bagno, C. Di Bello

Surface treatments and roughness properties of Ti-based biomaterials

J Mater Sci Mater Med, 15 (2004), pp. 935–949

[8]

X. Liu, P.K. Chu, C. Ding

Surface modification of titanium, titanium alloys, and related materials for biomedical applications

Mater Sci Eng R, 47 (2004), pp. 49–121

[9]

K. Duan, R. Wang

Surface modification of bone implants through wet chemistry

J Mater Chem, 16 (2006), pp. 2309–2321

[10]

G. Mendonça, D.B.S. Mendonça, F.J.L. Aragão, L.F. Cooper

Advancing dental implant surface technology – from micron- to nanotopography

Biomaterials, 29 (2008), pp. 3822–3835

[11]

A. Wennerberg, T. Albrektsson

On implant surfaces: a review of current knowledge and opinions

Int J Oral Maxillofac Implants, 24 (2009), pp. 63–74

[12]

D.M. Dohan Ehrenfest, P.G. Coelho, B.-S. Kang, Y.-T. Sul, T. Albrektsson

Classification of osseointegrated implant surfaces: materials, chemistry and topography

Trends Biotechnol, 28 (2009), pp. 198–206

[13]

L.T. de Jonge, S.C.G. Leeuwenburgh, J.G.C. Wolke, J.A. Jansen

Organic-inorganic surface modifications for titanium implant surfaces

Pharm Res, 25 (2008), pp. 2357–2369

[14]

V. Karageorgiou, D. Kaplan

Porosity of 3D biomaterial scaffolds and osteogenesis

Biomaterials, 26 (2005), pp. 5474–5491

[15]

G. Ryan, A. Pandit, D.P. Apatsidis

Fabrication methods of porous metals for use in orthopaedic applications

Biomaterials, 27 (2006), pp. 2651–2670

[16]

B. Otsuki, M. Takemoto, S. Fujibayashi, M. Neo, T. Kokubo, T. Nakamura

Pore throat size and connectivity determine bone and tissue ingrowth into porous implants: three-dimensional micro-CT based structural analyses of porous bioactive titanium implants

Biomaterials, 27 (2006), pp. 5892–5900

[17]

V.V. Divya Rani, L. Vinoth-Kumar, V.C. Anitha, K. Manzoor, M. Deepthy, V.N. Shantikumar

Osteointegration of titanium implant is sensitive to specific nanostructure morphology

Acta Biomater, 8 (2012), pp. 1976–1989

[18]

L. Gobbato, E. Arguello, I. Sanz Martin, C.E. Hawley, T.J. Griffin

Early bone healing around 2 different experimental, HA grit-blasted, and dual acid-etched titanium implant surfaces. A pilot study in rabbits

Implant Dent, 21 (2012), pp. 454–460

[19]

H.S. Alghamdi, R. Bosco, J.J.J.P. van den Beucken, X.F. Walboomers, J.A. Jansen

Osteogenicity of titanium implants coated with calcium phosphate or collagen type-I in osteoporotic rats

Biomaterials, 34 (2013), pp. 3747–3757

[20]

M. Haenle, T. Lindner, M. Ellenrieder, M. Willfahrt, H. Schell, W. Mittelmeier, et al.

Bony integration of titanium implants with a novel bioactive calcium titanate (Ca4Ti3O10) surface treatment in a rabbit model

J Biomed Mater Res Part A, 100A (2012), pp. 2710–2716

[21]

T.-K. Kwon, H.-J. Lee, S.-K. Min, I.-S. Yeo

Evaluation of early bone response to fluoride-modified and anodically oxidized titanium implants through continuous remove torque analysis

Implant Dent, 21 (2012), pp. 427–432

[22]

A.M. Ballo, et al.

Bone tissue reactions to biomimetic ion-substituted apatite surfaces on titanium implants

J R Soc Interface, 9 (2012), pp. 1615–1624

[23]

W. Zhang, et al.

The synergistic effect of hierarchical micro/nano-topography and bioactive ions for enhanced osseointegration

Biomaterials, 34 (2013), pp. 3184–3195

[24]

M. de Wild, et al.

Bone regeneration by osteoconductivity of porous titanium implants manufactured by selective laser melting: a histological and micro computed tomography study in the rabbit

Tissue Eng Part A (2013) http://dx.doi.org/10.1089/ten.tea.2012.0753

[25]

C. Zhao, X. Zhu, K. Liang, J. Ding, Z. Xiang, H. Fan, et al.

Osteoinduction of porous titanium: a comparative study between acid-alkali and chemical-thermal treatments

J Biomed Mater Res Part B: Appl Biomater, 95B (2010), pp. 387–396

[26]

Y.C. Chai, et al.

Ectopic bone formation by 3D porous calcium phosphate-Ti6Al4V hybrids produced by perfusion electrodeposition

Biomaterials, 33 (2012), pp. 4044–4058

[27]

U. Ripamonti, L.C. Roden, L.F. Renton

Osteoinductive hydroxyapatite-coated titanium implants

Biomaterials, 33 (2012), pp. 3813–3823

[28]

Q. Fu, Y. Hong, X. Liu, H. Fan, X. Zhang

A hierarchically graded bioactive scaffold bonded to titanium substrates for attachment to bone

Biomaterials, 32 (2011), pp. 7333–7346

[29]

A. Braem, T. Mattheys, B. Neirinck, J. Schrooten, O. Van der Biest, J. Vleugels

Porous titanium coatings through electrophoretic deposition of TiH2 suspensions

Adv Eng Mater, 13 (2011), pp. 509–515

[30]

S.K.L. Levengood, S.J. Polak, M.B. Wheeler, A.J. Maki, S.G. Clark, R.D. Jamison, et al.

Multiscale osteointegraton as a new paradigm for the design of calcium phosphate scaffolds for bone regeneration

Biomaterials, 31 (2010), pp. 3552–3563

[31]

O. Chan, et al.

The effects of microporosity on osteoinduction of calcium phosphate bone graft substitute biomaterials

Acta Biomater, 8 (2012), pp. 2788–2794

[32]

S. Polak, S.K.L. Levengood, M.B. Wheeler, A.J. Maki, S.G. Clark, A.J. Wagoner Johnson

Analysis of the roles of microporosity and BMP-2 on multiple measures of bone regeneration and healing in calcium phosphate scaffolds

Acta Biomater, 7 (2011), pp. 1760–1771

[33]

J.-M. Wu, S. Hayakawa, K. Tsuru, A. Osaka

Low-temperature preparation of anatase and rutile layers on titanium substrates and their ability to induce in vitro apatite deposition

J Am Ceram Soc, 87 (9) (2004), pp. 1635–1642

[34]

N. Drnovšek, N. Daneu, A. Rečnik, M. Mazaj, J. Kovač, S. Novak

Hydrothermal synthesis of a nanocrystalline anatase layer on Ti6Al4V implants

Surf Coat Technol, 203 (2009), pp. 1462–1468

[35]

Bouazza S, Fuchs E, Rosin A, Willert-Porada M, Synthesis and properties of graded porous Ti–TiO2 multifunctional composites obtained by different processing methods. In: Kawasaki A, Kumakawa A, Niino M, editors. 10th International Symposium on Multiscale, Multifunctional and Functionally Graded Materials, 22–25 September 2008, Sendai, Japan. Materials Science Forum, vol. 631–32. Zürich: Trans Tech; 2010. p. 141–46.

[36]

Y.-T. Sul, C.B. Johansson, Y. Jeong, A. Wennerberg, T. Albrektsson

Resonance frequency and removal torque analysis of implants with turned and anodized surface oxides

Clin Oral Impl Res, 13 (2002), pp. 252–259

[37]

L.-H. Li, Y.-M. Kong, H.-W. Kim, Y.-W. Kim, H.-E. Kim, S.-J. Heo, et al.

Improved biological performance of Ti implants due to surface modification by micro-arc oxidation

Biomaterials, 25 (2004), pp. 2867–2875

[38]

W.-H. Song, H.S. Ryu, S.-H. Hong

Apatite induction on Ca-containing titania formed by micro-arc oxidation

J Am Ceram Soc, 88 (2005), pp. 2642–2644

[39]

L.L. Hench

Bioceramics

J Am Ceram Soc, 81 (1998), pp. 1705–1728

[40]

P. Valerio, M.M. Pereira, A.M. Goes, M.F. Leite

The effect of ionic products from bioactive glass dissolution on osteoblast proliferation and collagen production

Biomaterials, 25 (2004), pp. 2941–2948

[41]

D. Arcos, M. Vallet-Regí

Sol-gel silica-based biomaterials and bone tissue regeneration

Acta Biomater, 6 (2010), pp. 2874–2888

[42]

A. Braem, B. Neirinck, J. Schrooten, O. Van der Biest, J. Vleugels

Biofunctionalisation of porous titanium coatings through sol-gel impregnation with a bioactive glass-ceramic

Mater Sci Eng C, 32 (2012), pp. 2292–2298

[43]

A. Chaudhari, A. Braem, J. Vleugels, J.A. Martens, I. Naert, M. Vivan Cardoso, et al.

Bone tissue response to porous and functionalized titanium and silica based coatings

PloS One, 6 (2011), p. e24186

[44]

Okamoto H, Hg (mercury) binary alloy phase diagrams. In: ASM Handbook, vol. 3: Alloy Phase Diagrams. Materials Park, OH: ASM, International; 1992.

[45]

E. Slaets, I. Naert, G. Carmeliet, J. Duyck

Early cortical bone healing around loaded titanium implants: a histological study in the rabbit

Clin Oral Impl Res, 20 (2009), pp. 126–134

[46]

R. Nedir, M. Bischof, J.M. Briaux, S. Beyer, S. Szmukler-Moncler, J.P. Bernard

A 7-year life table analysis from a prospective study on ITI implants with special emphasis on the use of short implants. Results from a private practice

Clin Oral Implants Res, 15 (2004), pp. 150–157

[47]

P.A. Fugazzotto

Success and failure rates of osseointegrated implants in function in regenerated bone for 72 to 133 months

J Oral Maxillofacial Implants, 20 (2005), pp. 77–83

[48]

M.A. Hartzband, A.H. Glassman, V.M. Goldberg, L.R. Jordan, R.D. Crowninshield, K.B. Fricka, et al.

Survivorship of a low-stiffness extensively porous-coated femoral stem at 10 years

Clin Orthop Relat Res, 468 (2010), pp. 433–440

[49]

J. Sanz-Reig, A. Lizaur-Utrilla, I. Llamas-Merino, F. Lopez-Prats

Cementless total hip arthroplasty using titanium, plasma-sprayed implants: a study with 10 to 15 years of follow-up

J Orthop Surg, 19 (2011), pp. 169–173

[50]

B.M. Willie, et al.

Osseointegration into a novel titanium foam implant in the distal femur of a rabbit

J Biomed Mater Res B Appl Biomater, 92 (2010), pp. 479–488

[51]

L. Le Guéhennec, A. Soueidan, P. Layrolle, Y. Amouriq

Surface treatments of titanium dental implants for rapid osseointegration

Dent Mater, 23 (2007), pp. 844–854

[52]

A. Braem, et al.

J. Staphylococcal biofilm growth on smooth and porous titanium coatings for biomedical applications

J Biomed Mater Res Part A (2013) http://dx.doi.org/10.1002/jbm.a.34688

[53]

K.A. Hing, B. Annaz, S. Saeed, P.A. Revell, T. Buckland

Microporosity enhances bioactivity of synthetic bone graft substitutes

J Mater Sci Mater Med, 16 (2005), pp. 467–475

[54]

P. Habibovic, H. Yuan, C.M. van der Valk, G. Meijer, C.A. van Blitterswijk, K. de Groot

3D microenvironment as essential element for osteoinduction by biomaterials

Biomaterials, 26 (2005), pp. 3565–3575

[55]

J. Malmström, E. Adolfsson, A. Arvidsson, P. Thomsen

Bone response inside free-form fabricated macroporous hydroxyapatite scaffolds with and without an open microporosity

Clin Impl Dent Relat Res, 9 (2007), pp. 79–88

[56]

A.I. Itälä, H.O. Ylänen, C. Ekholm, K.H. Karlsson, H.T. Aro

Pore diameter of more than 100 μm is not requisite for bone ingrowth in rabbits

J Biomed Mater Res, 58 (2001), pp. 679–683

[57]

L. Gan, J. Wang, A. Tache, N. Valiquette, D. Deporter, R. Pilliar

Calcium phosphate sol-gel-derived thin films on porous-surfaced implants for enhanced osteoconductivity. Part II: Short-term in vivo studies

Biomaterials, 25 (2004), pp. 5313–5321

[58]

R.M. Wazen, L.-P. Lefebvre, E. Baril, A. Nanci

Initial evaluation of bone ingrowth into a novel porous titanium coating

J Biomed Mater Res Appl Biomater, 94B (2010), pp. 64–71

[59]

E. Baril, L.P. Lefebvre, S.A. Hacking

Direct visualization and quantification of bone growth into porous titanium implants using micro computed tomography

J Mater Sci: Mater Med, 22 (2011), pp. 1321–1332

[60]

W. Cao, L.L. Hench

Genetic design of bioactive glass

J Eur Ceram Soc, 29 (2009), pp. 1257–1265

[61]

N. Olmo, A. Martín, A. Salinas, J. Turnay, M. Vallet-Regí, M. Lizarbe

Bioactive sol-gel glasses with and without a hydroxycarbonate apatite layer as substrate for osteoblast cell adhesion and proliferation

Biomaterials, 24 (2003), pp. 3383–3393